International Journal of Power and Energy Systems, Vol. 46, No. 10, 2026
An Open Access Paper

RESEARCH ON THERMAL CHARACTERISTICS AND OVERLOAD CAPACITY OF OFFSHORE CONVERTER TRANSFORMERS

Zheng Zhao,* Lingfei Xiong,* Kuan Zheng*

Abstract

As a core component of offshore flexible DC power transmission systems, the thermal characteristics and overload capacity of converter transformers have garnered significant attention. This study employs a field-circuit coupled calculation method that combines steady-state simulation and thermal circuit modeling to precisely evaluate these properties. Using Fluent, the temperature and flow fields of a 2D model are solved, examining the temperature-dependent variations in transformer oil's density, specific heat capacity, and thermal conductivity. These findings enhance the accuracy of thermal field simulations. Detailed descriptions of solid domain material properties and heat source configurations, including silicon steel, copper, and cellulose, are provided, along with heat flux density calculations for each low and high-voltage winding segment. Results indicate that the transformer's hot spot is at the low-voltage winding top, with the high-voltage winding's maximum temperature in the top segment, and the highest internal oil flow velocity at the internal baffle. The field-circuit coupled model, considering real-time requirements, demonstrates higher computational accuracy than standard methods through hotspot temperature calculations. These outcomes are highly valuable for improving the performance, reliability, and cost-effectiveness of offshore wind power transmission systems and advancing the sustainable growth of the offshore wind energy sector.

Key Words

Converter Transformer, Thermal Characteristics, Overload, Flow Field, Field-Circuit Coupling

1. Introduction

With the continuous tightness of global energy supply, all countries around the world have regarded the development of new energy industries as an important means to alleviate the contradiction between energy supply and demand. Among them, wind power generation is relatively mature compared to other new energy sources, with advantages such as not relying on other primary energy sources, no fuel price risk, stable operating costs, and no carbon emissions or other environmental costs. It has attracted the attention of countries around the world. With the large-scale development and utilization of onshore wind resources, offshore wind power has gained favor due to its advantages such as stable and continuous wind resources, high wind speed, large power generation, and no occupation of land resources. Moreover, offshore wind power is close to economically developed areas and is near the power load center, making it easier to integrate and consume wind power.

Against this background, the converter transformer in the offshore flexible direct current transmission system, as a key power equipment, has a large capacity and high voltage level. Its operational reliability has received increasing attention. The main function of the converter transformer in the power grid is the conversion between AC and DC power. Therefore, in addition to the AC sinusoidal component, there will also be harmonic components in the excitation current of the winding. Harmonic currents can cause the winding temperature to rise, increase harmonic losses, and eventually lead to local mechanical faults, thereby affecting the mechanical stability and reliability of the winding. Therefore, studying the thermal characteristics and overload capacity of the converter transformer winding is of great significance for ensuring the stable operation of the offshore wind power system.

References [1]-[5] have expounded on the thermal characteristics of the converter transformer under different operating conditions and established a temperature field model of the converter transformer, simulating and analyzing the temperature field characteristics of the converter transformer under multiple operating conditions. References [6]-[9] have studied the factors affecting the overload capacity of the converter transformer and, through parameter research, demonstrated the specific impact of these factors on the transformer's overload capacity, providing a basis for the safe operation, fault diagnosis, aging research,

* State Grid Economic Research Institute Co., Ltd., Beijing, China; e-mail: zhaozheng@chinasperi.sgcc.com.cn, xionglingfei@chinasperi.sgcc.com.cn, zhengkuan111@126.com
Corresponding Author: Kuan Zheng

Recommended by: Amirthagunaraj Yogarathnam
(DOI: 10.2316/J.2026.203-0642)

and cooling scheme design of the converter transformer.

Reference [10] considered the impact of the load signal of the converter transformer on its voice signal characteristics and selected the converter transformer of an 800 kV converter station as the research object. It collected fault signals including voice signals and current signals under overload conditions (such as DC bias) and constructed a sample library through historical playback. By introducing the load signal segmentation diagnosis interval, a joint feature vector was formed to improve the accuracy of fault diagnosis. The operation process of the converter transformer was divided into different load intervals, enabling the separate diagnosis of core faults and winding faults, effectively overcoming the problem of overlapping core and winding faults and improving the accuracy of fault identification.

Reference [11] detailly analyzed the operational capacity of the converter transformer under different overload conditions, including continuous overload, hour-level overload, and other states, and proposed corresponding calculation models and methods for each state. Under the continuous overload state, the transformer environment was built according to the designed wiring method, and the operational capacity data of the transformer under continuous overload conditions were collected and compared with the calculated values by the algorithm. The results showed that when the error was within ± 0.02p.u., the proposed algorithm met the calculation accuracy requirements. Statistical results indicated that when the transformer's operating environment temperature did not reach $25°C$, the operational capacity remained unchanged under continuous overload conditions; as the temperature increased, the operational capacity gradually decreased, and there was a linear relationship between the two. Under the hour-level overload state, different initial load rates (1.05p.u., 1.15p.u., 1.25p.u.) were used as analysis conditions, and the hour-level overload capacity was calculated using the proposed algorithm. The results showed that under different initial load rates, when the temperature remained constant, the overload capacity was positively correlated with the duration; when the initial load rate and overload capacity were the same, as the temperature increased, the duration gradually decreased. Under three initial load rate conditions, the overload capacity decreases as the initial overload rate increases, and the duration will also be shortened.

Reference [12] conducted an in-depth study on the vibration characteristics of ± 800 kV converter transformers under overload conditions. Through full-load thermal stability tests, important information such as vibration, voltage, and current under different load conditions was collected, and features such as vibration amplitude, vibration spectrum, main frequency, vibration power ratio in different frequency bands, vibration power entropy, and odd-even harmonic ratio were analyzed to evaluate the vibration state. Under overload conditions, the vibration amplitude of the converter transformer significantly increases, mainly due to the electromagnetic force generated by the load current in the windings. Theoretical analysis shows that the electromagnetic force is proportional to the square of the load current, so the vibration amplitude increases quadratically with the increase in the load rate. The vibration power ratio in different frequency bands changes, reflecting the shift of the vibration source from the core to the windings. The vibration power ratio in the low-frequency band (0-400 Hz) decreases from light load to medium load but increases from medium load to heavy load, while the opposite occurs in the high-frequency band. Under overload conditions, the vibration power entropy decreases, indicating a reduction in the complexity of the vibration signal. The odd-even harmonic ratio decreases with the increase in the load rate under overload conditions, which is related to the operating state of the filter.

Reference [13] analyzed the temperature distribution law of the windings of ± 800 kV converter transformers under the influence of different harmonic currents through a two-dimensional refined simulation model. It was pointed out that as the load rate increases, the vibration amplitude of the converter transformer significantly increases, mainly due to the electromagnetic force generated by the load current in the windings. The vibration frequency of the converter transformer gradually shifts from 200 Hz to 300 Hz or 400 Hz, indicating that under overload conditions, the vibration of the windings gradually replaces the vibration of the core as the dominant vibration source. In addition, the temperature rise caused by harmonic currents increases the hot spot temperature of the windings, thereby affecting the mechanical performance and stress distribution of the windings. High-frequency harmonic currents cause the equivalent resistance of the windings to gradually increase, intensifying the losses and further raising the temperature of the windings. Under overload conditions, the stress distribution and temperature distribution of the windings become more complex, and the coupling effect of harmonic currents and temperature rise needs to be comprehensively considered. The final research shows that as the content and frequency of harmonic currents increase, the hot spot temperature and stress of the windings significantly increase. The proposed winding stress calculation model can accurately reflect the influence of harmonic currents and temperature rise on the stress of the windings, providing important technical guidance for the design and maintenance of converter transformers.

Reference [14] studied the stress distribution characteristics of the windings of ± 800 kV converter transformers under the influence of harmonic currents through simulation, revealing the thermal characteristics and stress changes of the transformer under overload conditions. The research shows that harmonic currents cause the temperature of the windings to rise, with uneven temperature distribution, and the hot spots are mainly concentrated in the upper part of the windings. Under 250 Hz harmonics, as the harmonic current content increases from 0% to 20%, the hot spot temperature of the grid side winding rises from $87.2°C$ to $99.2°C$, and that of the valve side rises from $98.1°C$ to $108.7°C$; under 650 Hz harmonics, the temperature rise of the grid side hot spot is more significant. At the same time, the stress distribution of the

windings is affected by temperature and shifts towards the oil channels and the center area of the windings, with the maximum stress increasing in a power function relationship with the harmonic current content. The research also shows that the temperature rise caused by harmonic currents increases the equivalent resistance of the windings, intensifying losses and temperature rise, and the changes in stress distribution and magnitude reflect the complex mechanical behavior of the windings under overload conditions. These findings provide key guidance for the design and maintenance of converter transformers under overload conditions[15]-[16].

Therefore, to further enhance the performance, reliability and economy of the flexible DC transmission system for offshore wind power, and to support the development and construction of offshore wind power and contribute to the realization of China's dual carbon goals, in-depth research on the thermal characteristics and overload capacity of offshore converter transformers can improve the operational efficiency and reliability of converter transformers, and also ensure the efficient transmission of wind power and the guarantee of power quality. This is of great practical significance and urgency for promoting the rapid development of the offshore wind power industry.

2. Theoretical Research

To simulate the thermal and flow fields within a transformer, this study uses Fluent, a numerical calculation software based on the finite volume method. The physical foundation of this method is detailed below. Before numerical computation, the computational domain is divided into several control volumes. Each mesh point is surrounded by a control volume ΔV, the smallest geometric unit for applying control equations. The 2D structured mesh used in this study is shown in the figure below. In the figure, P represents the grid node under study and its surrounding control volume. The boundaries of this control volume are denoted as n, w, s, and e, with horizontal and vertical widths of Δx and Δy, respectively. N, W, S, and E represent the grid nodes adjacent to P and their surrounding control volumes.

Discretizing the conservative control equations of the finite volume method on each mesh yields:

$$\frac{\partial(\rho\varphi)}{\partial\tau}+\frac{\partial(\rho u\varphi)}{\partial x}+\frac{\partial(\rho v\varphi)}{\partial y}=\frac{\partial}{\partial x}(\Gamma\frac{\partial\varphi}{\partial x})+\frac{\partial}{\partial y}(\Gamma\frac{\partial\varphi}{\partial y})+S \quad (1)$$

The equation can be divided into four parts, representing the sum of the rate of change of a general variable φ with time, and the convective outflow equals the sum of the diffusive inflow and the increase from internal sources. As this study focuses on steady-state results, the first term on the left, the partial derivative with respect to time, is zero. u and v denote the velocity components of φ in the x and y directions, Γ is the diffusion coefficient of φ, and S is the source term. Integrating the differential equation over each mesh gives:

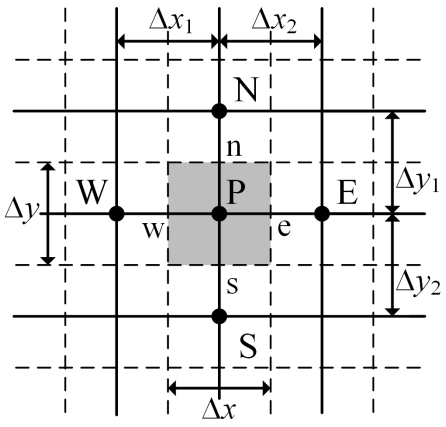

Figure 1. Two-dimensional structural mesh

$$\int_{\Delta V}\frac{\partial(\rho u\varphi)}{\partial x}+\int_{\Delta V}\frac{\partial(\rho v\varphi)}{\partial y}=\int_{\Delta V}\frac{\partial}{\partial x}(\Gamma\frac{\partial\varphi}{\partial x})+\int_{\Delta V}\frac{\partial}{\partial y}(\Gamma\frac{\partial\varphi}{\partial y})+\int_{\Delta V}S \quad (2)$$

Since $\Delta x_1=\Delta x_2=\Delta x$, $\Delta y_1=\Delta y_2=\Delta y$,
$\Delta V=\Delta x\Delta y$ the above equation can be expanded as:

$$\begin{aligned}&[(\rho u\varphi A)_e-(\rho u\varphi A)_w]+[(\rho v\varphi A)_n-(\rho v\varphi A)_x]\\&=\left[\left(\Gamma A\frac{\partial\varphi}{\partial x}\right)_e-\left(\Gamma A\frac{\partial\varphi}{\partial x}\right)_v\right]+\left[\left(\Gamma A\frac{\partial\varphi}{\partial y}\right)_n-\left(\Gamma A\frac{\partial\varphi}{\partial y}\right)_x\right]\\&\quad+S\Delta x\Delta y\end{aligned} \quad (3)$$

Where the convection term and diffusion term are represented by the convection flow rate and diffusion quantity at the control volume boundary, A represents the length of the control volume boundary, and the subscripts e, w, n, and s pass through the eastern, western, northern, and southern boundaries, respectively. And $A_w=A_e=\Delta x, A_n=A_s=\Delta y$. These quantities can be further represented by interpolating adjacent nodes in the difference-in-center format:

$$(\rho u\varphi A)_e=(\rho u)_eA_e\frac{\varphi_E+\varphi_P}{2} \quad (4)$$

$$(\rho u\varphi A)_w=(\rho u)_wA_w\frac{\varphi_W+\varphi_P}{2} \quad (5)$$

$$(\rho v\varphi A)_n=(\rho v)_nA_n\frac{\varphi_N+\varphi_P}{2} \quad (6)$$

$$(\rho v\varphi A)_s=(\rho v)_sA_s\frac{\varphi_S+\varphi_P}{2} \quad (7)$$

$$\left(\Gamma A\frac{\partial\varphi}{\partial x}\right)_e=\Gamma_eA_e\left[\frac{\varphi_E-\varphi_P}{\Delta x_2}\right] \quad (8)$$

$$\left(\Gamma A\frac{\partial\varphi}{\partial x}\right)_w=\Gamma_wA_w\left[\frac{\varphi_P-\varphi_W}{\Delta x_1}\right] \quad (9)$$

$$\left(\Gamma A\frac{\partial\varphi}{\partial x}\right)_n=\Gamma_nA_n\left[\frac{\varphi_N-\varphi_P}{\Delta y_1}\right] \quad (10)$$

$$\left(\Gamma A\frac{\partial\varphi}{\partial x}\right)_s=\Gamma_sA_s\left[\frac{\varphi_P-\varphi_S}{\Delta y_2}\right] \quad (11)$$

$$\begin{cases} F_i = (\rho u)_i A_i & \text{or } F_j = (\rho v)_j A_j \\ D_i = \dfrac{\Gamma_i A_i}{\Delta x_i} & \text{or } D_j = \dfrac{\Gamma_j A_j}{\Delta y_j} \end{cases} \tag{12}$$

where i takes w and e, and j takes n and s. Finishing is available:

$$\begin{aligned} &\left[\frac{F_e}{2}(\varphi_E + \varphi_P) - \frac{F_w}{2}(\varphi_W + \varphi_P)\right] + \left[\frac{F_n}{2}(\varphi_N + \varphi_P)\right. \\ &\left. - \frac{F_s}{2}(\varphi_S + \varphi_P)\right] = [D_e(\varphi_E - \varphi_P) - D_w(\varphi_P - \varphi_W)] \\ &+ [D_n(\varphi_N - \varphi_P) - D_s(\varphi_P - \varphi_S)] + S_V \end{aligned} \tag{13}$$

Based on the above equation, it is sorted out according to the general variable φ to obtain:

$$\begin{aligned} &\left[\left(D_e + \frac{F_e}{2}\right) + \left(D_w - \frac{F_w}{2}\right) + \left(D_n + \frac{F_n}{2}\right)\right. \\ &\left. + \left(D_s - \frac{F_s}{2}\right)\right]\varphi_P = \left(D_e - \frac{F_e}{2}\right)\varphi_E + \left(D_w + \frac{F_w}{2}\right)\varphi_W \\ &+ \left(D_n - \frac{F_n}{2}\right)\varphi_N + \left(D_s + \frac{F_s}{2}\right)\varphi_S + S_V \end{aligned} \tag{14}$$

The $\alpha = D \pm \frac{F}{2}$ coefficient of the variable of the normalized treatment is written:

$$\begin{aligned} \alpha_P \varphi_P &= \alpha_E \varphi_E + \alpha_W \varphi_W + \alpha_N \varphi_N + \alpha_S \varphi_S \alpha_P \\ &= \alpha_E + \alpha_W + \alpha_N + \alpha_S + F_E - F_W + F_N \\ &- F_S - S_P \end{aligned} \tag{15}$$

Write the discrete equation for all control node columns, and solve the system of equations according to the initial conditions to obtain the quantity to be solved.

3. Material Properties and Finite Element Simulation

To solve the temperature and flow fields of a 2D model using Fluent, it is essential to first specify the materials and their physical properties within the computational domain and accurately calculate the losses of heat-generating components.

3.1 Transformer Oil Physical Parameters

The oil-immersed transformer uses mineral oil as the cooling medium, and its physical properties, such as density ρ, specific heat capacity C_p, thermal conductivity γ, and dynamic viscosity, μ, will change with the change of temperature, affecting its heat transfer efficiency and heat dissipation effect. Therefore, the following laws of transformer oil physical parameters with temperature are summarized and set accordingly in the simulation model, which can improve the calculation accuracy of thermal field steady-state simulation.

a) Density

Based on the density of transformer oil measured at 5 K (5°C) intervals within the temperature range of 278.15 K (5°C) to 373.15 K (100°C), the density as a function of temperature is shown in Fig. 2 below. It can be seen from the figure that the density of transformer oil is approximately negatively linearly correlated with temperature, and the density decreases with the increase of temperature.

$$\rho(T) = 1093 - 0.826T + 3.612 \times 10^{-4} T^2 \left(\text{ kg} \cdot \text{ m}^{-3}\right) \tag{16}$$

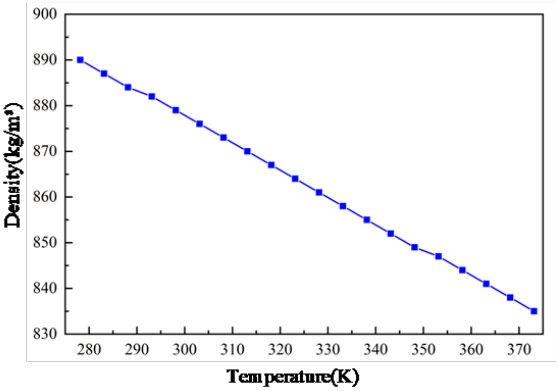

Figure 2. The Relationship Between Density and Temperature

According to the known data, the function relationship between density and temperature is obtained as follows, where ρ the transformer oil density is the transformer oil density and T is the oil temperature, which is only valid in the temperature range of $278.15 - 373.15$ K.

b) Specific heat capacity

Specific heat capacity is a commonly used physical quantity in thermodynamics, which refers to the energy absorbed or dissipated by a unit temperature of a unit mass of a substance rising or falling, and can be used to characterize the ability of the substance to absorb heat or dissipate heat. The specific heat capacity-temperature curve is shown in Fig. 3 using the specific heat capacity of the transformer oil corresponding to each 5 K interval in $278.15 - 373.15$ K.

$$C_p(T) = 455.9 + 5.191T - 1.522 \times 10^{-3} T^2 (\text{J} \cdot \text{kg}^{-1} \cdot \text{K}^{-1}) \tag{17}$$

From the curve, it can be seen that the two are approximately positively linearly correlated, and the specific heat capacity of transformer oil increases with the increase of temperature. After the function fitting, the functional relationship between the specific heat capacity and the temperature is obtained as follows, where C_p is the specific heat capacity of transformer oil. It is also noted that the equation holds only in the temperature range of $278.15 - 373.15$ K.

c) Thermal conductivity

Thermal conductivity characterizes the thermal conductivity of a material. The higher the thermal conductivity, the better the thermal conductivity of the material. According to the thermal conductivity of the transformer oil corresponding to each interval of 5

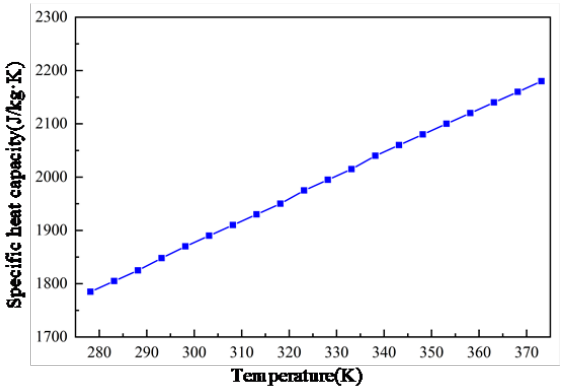

Figure 3. The Relationship Between Specific Heat Capacity and Temperature

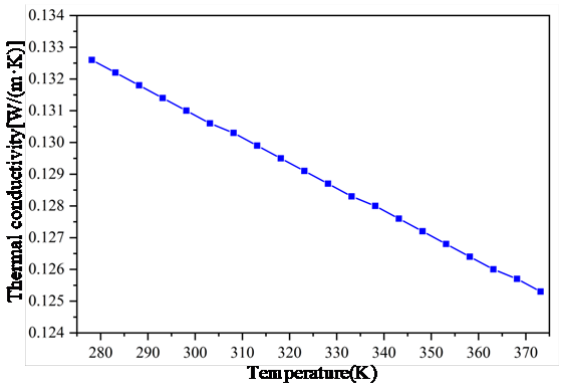

Figure 4. The Relationship Between Thermal Conductivity and Temperature

K in $278.15 - 373.15$ K, the curve of thermal conductivity with temperature as shown in Fig. 4 below is obtained.

The thermal conductivity of transformer oil decreases approximately linearly as the temperature rises. The relationship between thermal conductivity and temperature is fitted exponentially to obtain the functional relationship described in the following equation. In the following formula, is the thermal conductivity of transformer oil. This formula holds only when the temperature is in the range of 278.15 373.15 K.

$$\gamma(T) = 0.1538 - 7.645 \times 10^{-5} T(\mathrm{W \cdot m^{-1} \cdot K^{-1}}) \quad (18)$$

3.2 Solid Domain Material Characteristics and Heat Source Setting

The main materials used in the solid domain are silicon steel sheet, copper and cellulose, and their physical properties fluctuate very little in the temperature range of $273.15 - 373.15$ K, which can be regarded as constant in the simulation calculation:

$$\begin{aligned}
\rho_{fe} &= 7550(\ \mathrm{kg/m^3}) C_{pfe} \\
&= 446(\ \mathrm{J \cdot\ kg^{-1} \cdot\ K^{-1}}) \gamma_{fe} = 51.9(\ \mathrm{W \cdot m^{-1} \cdot\ K^{-1}}) \\
\rho_{cu} &= 8978(\ \mathrm{kg/m^3}) C_{pcu} \\
&= 381(\ \mathrm{J \cdot\ kg^{-1} \cdot\ K^{-1}}) \gamma_{cu} = 387.6(\ \mathrm{W \cdot m^{-1} \cdot\ K^{-1}}) \\
\rho_{isl} &= 1400(\ \mathrm{kg/m^3}) C_{pisl} \\
&= 1600(\ \mathrm{J \cdot\ kg^{-1} \cdot\ K^{-1}}) \gamma_{isl} = 0.15(\ \mathrm{W \cdot m^{-1} \cdot\ K^{-1}})
\end{aligned}$$

Among them, the subscripts Fe, Cu and ISL represent the iron core, copper wire, and insulating paper composed of the above materials, respectively.

The winding is composed of two parts, copper wire and insulating paper, when calculating the calorific value per unit volume of low-voltage and high-voltage windings, it is necessary to consider the influence of insulating paper, and multiply the heat source per unit volume of the copper conductor by the area ratio of the copper conductor to the wire cake in the two-dimensional model, so as to obtain the equivalent unit volume heat source of the wire cake. In addition, the cushion block between the wire cake and the wire cake is not conducive to the heat dissipation of the winding, and the equivalent volume heat source needs to be adjusted according to the coverage area, and finally the heat flux density of each wire cake of the low-voltage and high-voltage windings is 247.4 kW/m3 and 181.6 kW/m3, respectively.

3.3 Boundary Condition Setting and Model Selection

The interaction between the fluid and the wall is the key to the coupling heat transfer problem, and the appropriate boundary conditions and initial conditions can not only meet the thermophysical requirements but also improve the stability of the calculation. According to the actual situation of the temperature rise test, the ambient temperature was set to 293.15 K in the simulation. All solid surfaces in contact with the oil are non-slip, the outer surface of the oil tank and radiator is set to convective heat transfer, and the thermal boundary conditions of the rest of the solid surfaces are coupled heat transfer. In order to ensure the convergence and stability of the calculation, two criteria are used to determine that the temperature field and flow field in the transformer reach a steady state, one is that the residuals of these equations are within the allowable range: the residuals of the continuity and velocity equations are less than 10^{-3}, and the residuals of the energy equations are less than 10^{-6}; Another criterion is that the area-weighted average temperature fluctuation of the low-voltage winding is less than 0.5°C in 1000 step iterations.

The proper selection of the mathematical model should first judge the type of oil flow in the transformer, and the main judgment is based on the Reynolds number. Usually, the Reynolds number less than 2300 is laminar flow, otherwise it is considered turbulence. For ON-type transformers, the oil flow velocity is very low (oil flow inlet ve-

locity less than 0.1 m/s), and the kinematic viscosity is high, resulting in a low Reynolds number for the flow. In the two-dimensional model established in this paper, the Reynolds number is estimated to be about 31 based on the temperature, flow velocity, and channel width of the oil inlet, so the laminar flow model is adopted. In addition to this, in order to facilitate the calculation of fast convergence, the pressure solver chooses PRESTO based on staggered volume control.

3.4 Model Simulation Results

Taking the DF-80000/220 transformer as an example, the model information is shown in Table 1. Among them, " $230/\sqrt{3}$kV " refers to the rated phase voltage of the high-voltage winding (Y-connection), and " 35 kV " refers to the rated line voltage of the low-voltage winding (Δ-connection). After running 15,000 steps in Fluent, the steady-state convergence result was obtained. In the simulation model, no heat source load is applied to the core part, and the equivalent heat source power of eddy current loss is set for the top and bottom wire cakes of the high and low voltage windings. The cooling method of the transformer follows the IEC 60076-7 standard, where the acronym ONAF (Oil Natural Air Forced) describes the cooling system characterized by natural oil circulation combined with forced air cooling via fans.

Table 1
Transformer Model Information

Transformer model	Cooling method	Rated voltage /kV	Rated capacity/kVA
DF- 80000/220	ONAF	$230/\sqrt{3}/35$	80000

Figure 5 visualizes the operational thermal profile: (a) presents the full transformer with temperature gradients, revealing hotspots at the core-stack junction and upper windings; (b) zooms into the high-voltage winding, where the peak temperature at the top terminal correlates with current concentration in the terminal assembly. As can be seen from Fig.5, the hot spot temperature of the transformer is 108.1°C, which appears at the top of the low-voltage winding, and the maximum temperature of the high-voltage winding is 97.88°C, which appears in the high-voltage winding top line cake. The internal temperature distribution and hot spot position of the transformer winding are different from those of the previous two, which is analyzed to be caused by the large eddy current loss of the wire cake at the top of the winding. In the vicinity of the oil baffle inside the winding, the temperature distribution also presents a more obvious local extreme phenomenon.

Figure 6 visualizes the oil flow dynamics: (a) presents the full transformer with velocity gradients, highlighting high-velocity channels at the oil inlet and low-velocity recirculation zones near the corelamination interface; (b) zooms into the high-voltage winding region, where the peak flow velocity at the winding entrance corresponds to the structural design of the internal oil ducts. The maximum oil flow rate inside the transformer is 0.102 m/s, and

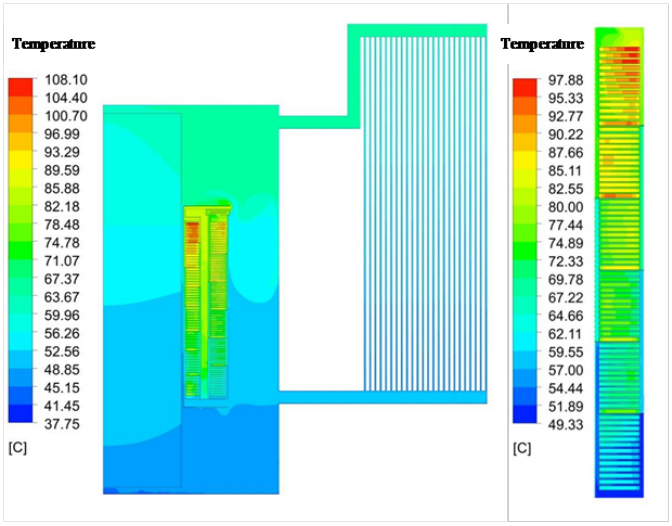

Figure 5. Transformer Temperature Distribution Cloud Map

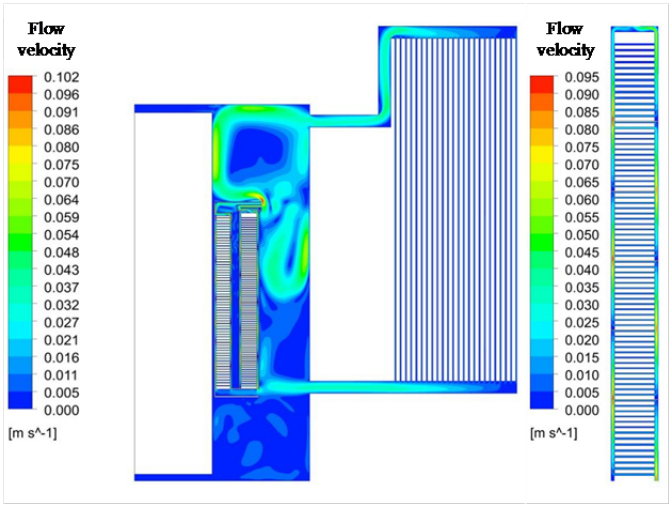

Figure 6. Cloud Map of Transformer Oil Flow Velocity Distribution

the maximum oil flow rate of the high-voltage winding is 0.095 m/s, which appears at the internal oil baffle.

3.5 Simulation Model and Solution Process of Converter Transformer Temperature Field

(1) Analysis of harmonic influence on the temperature field of the converter transformer and study on copper shielding effect
The finite element analysis software is used to calculate the temperature of the converter transformer, and the Joule heat obtained in the magnetic field is used as the thermal load of the temperature field analysis, which is applied to the transformer winding and its oil tank, and structural parts, respectively. At the same time, the changes of the hot spot temperature of the converter transformer winding, the hot spot temperature of the oil tank wall, and the hot spot temperature of the clamp before and after the installation of the cop-

Table 2
Thermal Properties of Converter Transformer Structural Parts

Component	Material	Permeability	Thermal conductivity W/ (m · °C)	Specific heat capacity J/ (kg · ° C)	Density (kg/m^3)
Core	27ZH100	B-H curve	21 m · °C	490 kg · °C	7650 kg/m^3
Winding	Copper	-	338	381	8978
Oil tank	A3 Steel	B-H curve	50	485	7800
Clamping	Nonmagnetic steel	-	50	502	8030

per shield under the harmonic condition are analyzed. Table 2 shows the thermal properties of the converter transformer core, winding, oil tank, and clamp.

The converter valve generally uses a 12 -pulse valve group. Due to the rapid conversion of the on-off valve during the working process of the converter valve, many harmonics will be generated, which have a significant impact on the quality of the power supply. Since the 12-pulse converter valve group is composed of two 6-pulse converters in series, it is generally studied by analyzing the 6-pulse converter valve as an example. The function of the converter determines that many harmonics will be generated during the commutation process. The types of harmonics can be roughly divided into three categories: characteristic harmonics, non-characteristic harmonics, and conduction harmonics.

For the 12 -pulse rectifier, the $6 \times (2\ \mathrm{K} - 1) \pm 1$ harmonics cancel each other due to the equal amplitude of each harmonic component of the Y/y and Y/d converter transformers and the same phase of the 12 K+1 harmonics. Therefore, there are only characteristic harmonics in the 6-pulse harmonics, of which $6\ \mathrm{K} + 1$ is a positive-sequence characteristic wave and $6\ \mathrm{K} - 1$ is a negative-sequence characteristic wave. Therefore, there are only $12\ \mathrm{K} + 1$ harmonics on the AC side of the 12 -pulse converter.

In the process of engineering operation, there is a certain gap between the operation of DC transmission project and the theoretical simulation state. Therefore, there are other ripples accompanied by characteristic harmonics, which are called non-characteristic harmonics. Such harmonics are often caused by non-ideal conditions. For example, the trigger pulse period is not absolutely equal, the bus voltage is not strictly symmetrical or the commutation reactance is unbalanced, which may lead to the generation of non-characteristic harmonics. Due to the many and complex causes of non-characteristic harmonics, and in the actual equipment manufacturing process, manufacturers will specifically design to maximize the suppression of non-characteristic harmonics, so that the impact of non-characteristic harmonics in the DC transmission process is not obvious. The analysis of non-characteristic harmonics often adopts the method of ignoring other causes and analyzing a certain cause.

(2) Field-circuit coupling model of converter transformer

The single capacity of the ultra-high voltage converter transformer is large, so the stray loss caused by the leakage magnetic field is becoming more serious, and it will undoubtedly increase the stray loss caused by the leakage magnetic field in the case of DC bias or serious harmonics. Therefore, this chapter will carry out finite element simulation calculation on the hot spot temperature of converter transformer winding, oil tank wall and clamp under harmonic conditions, and compare it with the temperature after adding copper shielding.

Fig. 7 is a 1/2 converter transformer three-dimensional model diagram based on the converter transformer model ZZDFPZ-412300/750-200 provided by the transformer company. Based on the parameters of the transformer experimental model, the transformer model is simplified. Due to the symmetry, half of the three-dimensional physical model and equivalent circuit model are established by MAGNET software, which is the field-circuit coupling model, as shown in Fig.8.

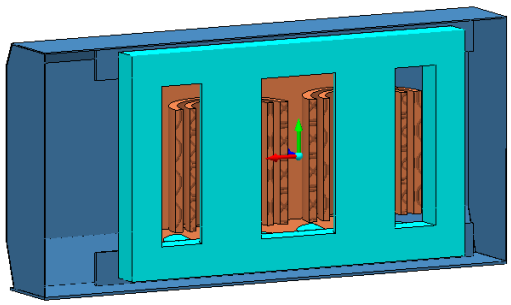

Figure 7. 1/2 Structure Model Diagram of Converter Transformer

(3) Solution process

According to the finite element simulation model established above, the corresponding material properties are loaded into the physical model, and the accuracy suitable for this simulation is selected for subdivision. The corresponding subdivision results are shown in Fig.9. According to the field-circuit coupling method, the physical model of the transformer is coupled with the circuit model, and the relevant simulation analysis is carried out. A sinusoidal AC voltage source is added to the primary side of the circuit model, and the equivalent simulation calculation is performed on the working conditions under harmonics. The initial temperature of the environment was set to 30°C.

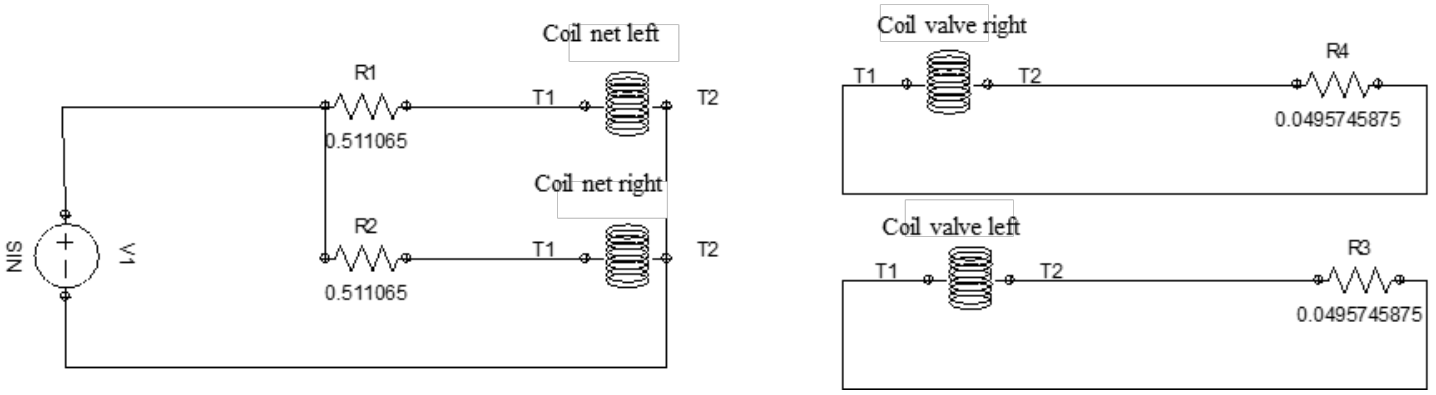

Figure 8. Field-Circuit Coupling Model

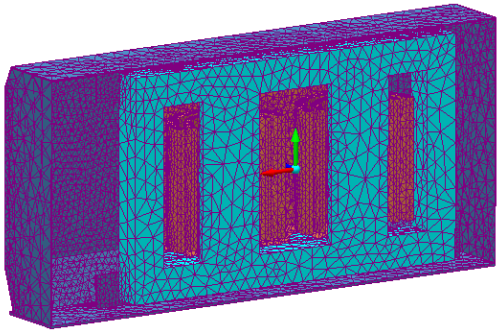

Figure 9. Meshing Diagram of the Model

Compared with the general transformer, the structure of the converter transformer is more complex, and its interior has a variety of media and nonlinear materials. Therefore, this chapter uses MagNet/ThermNet electromagnetic field finite element analysis software. According to the symmetry of the converter transformer structure and the characteristics of the electromagnetic distribution, the calculation model of the converter transformer is simplified and assumed as follows:

(1) Because the converter transformer is a symmetrical structure, so the calculation reduces the calculation time to take the model of the whole transformer 1/2 structure, and the inner side of the symmetrical surface is set to a symmetrical boundary.
(2) Ignoring the DC component of the low-voltage valve side winding, the total ampere turns of the grid side winding and the valve side winding are balanced after considering the influence of the high-order harmonic current.
(3) The core silicon steel sheets and components of the converter transformer are processed according to the nonlinear material of the non-magnetic steel, ignoring the hysteresis effect of the ferromagnetic material and being isotropic.
(4) Ignore the eddy current in the core, and the influence of lead current and displacement current on the leakage magnetic field.

According to the above solution process, the core loss of the converter transformer in MagNet under no-load condition is 166 kW and the load loss is 1050 kW. Fig. 10, Fig. 11 and Fig. 12 show the unshielded temperature of the converter transformer and the temperature distribution of the tank wall and the clamp under rated conditions.

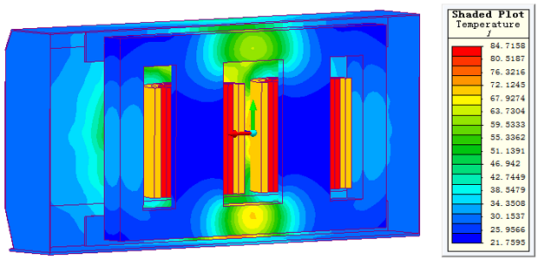

Figure 10. The Overall Temperature Distribution Cloud Diagram of the Transformer

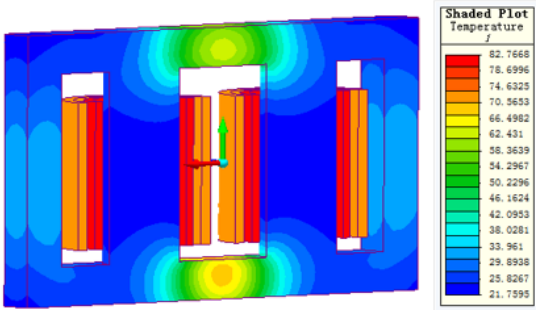

Figure 11. Temperature Distribution Cloud Diagram of Core and Winding

As shown in Fig.10, Fig. 11 and Fig.12, before the magnetic shielding is not installed, the hot spot temperature of the winding can reach 82.77°C, and the hot spot temperature of the core can reach 74.92°C. The eddy current density of the fuel tank is concentrated at the hot spot of the winding corresponding to the rear wall of the fuel tank, reaching 84.72°C. The clamp is located in the area where the leakage magnetic field of the transformer is strong, and the size is relatively small compared with other structural parts. It is easy to induce a large eddy current loss in its local area. The highest temperature rise of the clamp is at the central column of the iron core, because this is a

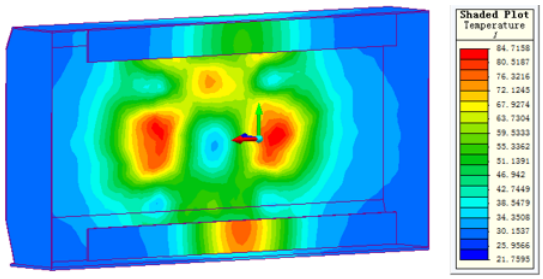

Figure 12. Temperature Distribution Cloud Diagram of Fuel Tank Wall and Clamp

high magnetic flux leakage area, and the eddy current loss is relatively large, so the temperature rise here is higher, forming a local hot spot, and at this time the hot spot temperature of the clamp also reached 77.52°C.

The heat resistance grade of oil-immersed transformers is grade A, and the insulation materials used in the transformer have a certain heat resistance life. At this time, the hot spot temperature of the oil tank wall and the hot spot temperature of the clamp will form local overheating. Therefore, this local overheating will cause insulation aging, threatening the safe use and life of the transformer, and it must be improved. Electromagnetic shielding generally refers to the shielding device made of a copper plate (or an aluminum plate), and the installation of electromagnetic shielding in the fuel tank is one of the main methods commonly used in engineering to reduce the eddy current loss caused by magnetic flux leakage on the fuel tank. Under the action of the magnetic flux of the leakage magnetic field, an eddy current will be induced on the surface of the copper plate. The magnetic field generated by the eddy current is just opposite to the direction of the leakage magnetic field and cancels each other out, so that the leakage magnetic flux entering the transformer tank is reduced, so as to achieve the purpose of reducing the eddy current loss and magnetic flux density of the transformer tank. In view of the above problems, this paper adds a 4mm thick copper shield in the calculation.

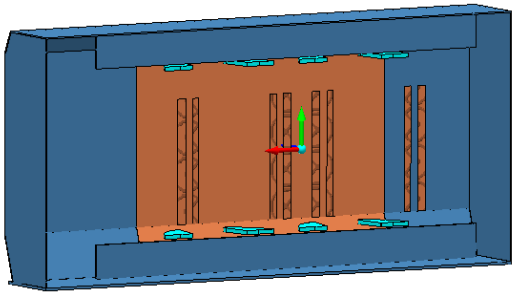

Figure 13. Copper Shielding Position Structure Diagram

After adding copper shielding in the simulation, the temperature field of the current transformer under rated load is simulated to verify the influence of copper shielding on high temperature. Fig. 14 and Fig. 15 are shown as the core, winding temperature cloud map, fuel tank wall, and clamp temperature cloud map after the installation of the copper shield.

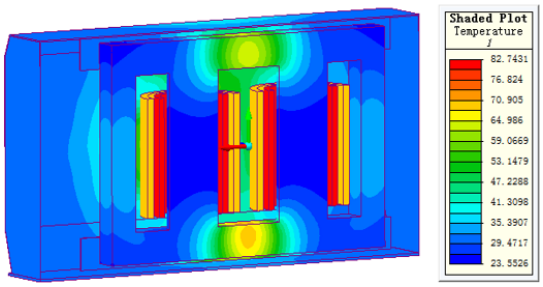

Figure 14. Cloud Map of Core and Winding Temperature Distribution

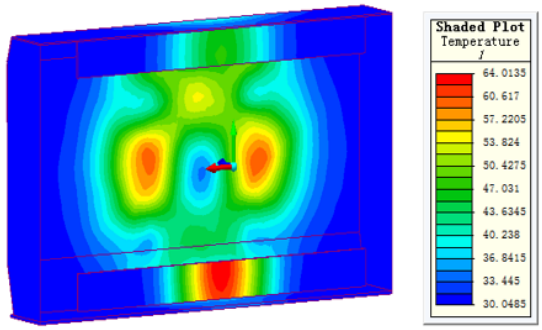

Figure 15. Cloud Map of Temperature Distribution on the Fuel Tank Wall and Clamps

After the installation of 4 mm thick copper shield, from Fig.15, the hot spot temperature of the fuel tank drops to 60.52°C, and the hot spot temperature of the clamp drops to 64.01°C. The calculated temperature rise conforms to the temperature rise limit of Class A insulating material. Therefore, the copper shields installed in the following parts of this section are all 4 mm thick.

4. Thermal Rise Calculation Considering Accuracy and Real-Time Requirements

The thermal circuit model method, while fast and simple, has lower accuracy due to parameter errors from simplified heat transfer representations. In contrast, the steady-state simulation method offers high accuracy and detailed physical field distributions but is computationally intensive and time-consuming, requiring significant computer resources and making it less practical for on-site use. To reconcile the need for both accuracy and real-time performance, a field-circuit coupling method is proposed. This method refines the thermal circuit model parameters based on simulation results, enabling precise hotspot temperature calculations.

For the field-circuit coupling model, the first step is to identify the coupling parameters. These parameters are categorized into five classes, as shown in Fig.16. Nameplate data, structural data, and winding DC resistance can be obtained from routine transformer tests. Temperature-rise test data, used to simplify heat dissipation resistance

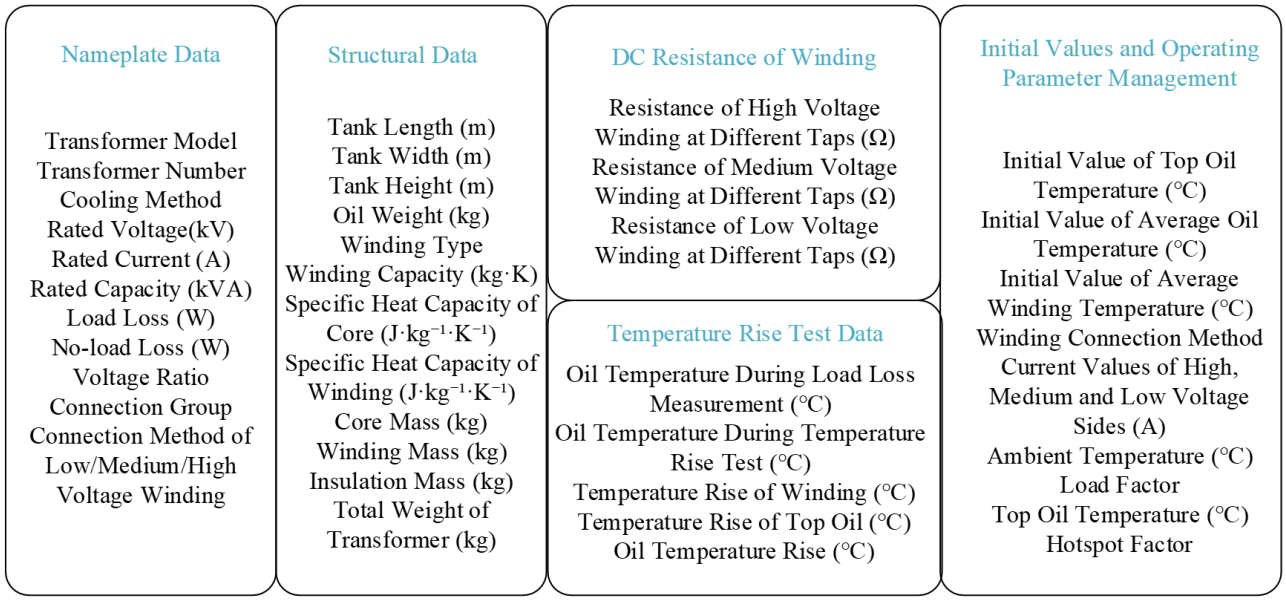

Figure 16. Parameters Required for the Hot Path Model Method

calculations, are derived from temperature-rise tests; if these tests are unavailable, relevant data such as the number and height of coils in different windings and the outer/inner diameters of windings can be used as alternatives. When the transformer tap position is fixed, these data remain unchanged for each calculation. Initial value data, which affect the speed of the thermal circuit model method, can be roughly estimated due to the method's fast computation speed. Operating data, which vary with the transformer's operating state, directly impact calculation accuracy. Ambient temperature and load current can be monitored in real-time, while top oil temperature and hotspot coefficients require precise assignment.

For transformers with online top-oil-temperature monitoring, real-time top-oil-temperature data is accessible. However, installing temperature sensors inside transformers demands high design standards for internal structures, and most transformers lack these sensors. Retrofitting in-service transformers with sensors is more challenging and costly than installing them during design or manufacturing. The hot-spot coefficient lacks a precise definition formula. Load guidelines suggest a hot-spot coefficient of 1.3 for medium and large transformers, yet this approach overlooks the specific structure and operating conditions of transformers, potentially compromising the accuracy of hot-spot temperature calculations. steady-state simulation can model the steady thermal field of transformers under any operating conditions, allowing for the calculation of the top-oil temperature and hot-spot coefficient. Based on this, the coupling parameters of the thermal circuit model and steady-state simulation are identified as the top-oil temperature and hot-spot coefficient.

The core steps of the coupled calculation model are as follows:1. Use steady-state simulation to model the operation of the transformer under typical load currents and ambient temperatures. Collect data on top-oil temperature, bottom-oil temperature, hot-spot temperature, and average winding temperature under different operating conditions to calculate the hot-spot coefficient and form a database.2. Analyze the database to determine the relationship between top-oil temperature, hot-spot coefficient, load ratio, and ambient temperature. Develop formulas for calculating top-oil temperature and hot-spot coefficient under any load and ambient temperature conditions.3. During field operation of the transformer, calculate the top-oil temperature and hot-spot coefficient based on actual operating conditions and input them into the thermal circuit model. This enables quick estimation of the hot-spot temperature at steady-state and supports simulation calculations. The following Fig. 17 summarizes the above approach. Taking the SFZ8-31500/110 transformer as an example, the first two steps are described in detail.

(1) The general provisions of power transformers stipulate that the maximum ambient temperature of power transformer operation shall not exceed 40°C, the minimum ambient temperature of indoor transformer operation shall not be less than −5°C, and the minimum ambient temperature of outdoor transformer shall not be less than −25°C. Considering that users are more concerned about the change of the internal temperature of the transformer at high temperatures, when the ambient temperature is very low, the temperature rise of the windings is small even at high load rates, so the ambient temperature range of steady-state simulation is set at 5°C ∼ 40°C (simulated every 5°C). Generally, the economic load rate of the transformer is 0.75 ∼ 0.85, when the transformer needs to bear the overload, the load rate should not exceed 1.2, considering that some in-service transformers have a long operating life and the carrying capacity is reduced, the range of load rate selected in the steady-state simulation is 0.4 ∼ 1.2 (every 0.2 simulation). Since the hot

Table 3
Top Oil Temperature and Hot Spot Coefficient of Transformers Under Different Operating Conditions

Load rate	**Ambient temperature**	0.4	0.6	0.8	1.0	1.2
5°C	Top layer oil temperature /°C	27.18	30.85	38.11	47.10	55.03
	Hot Spot Coefficient	1.29	1.31	1.26	1.17	1.16
10°C	Top layer oil temperature/ °C	30.31	35.90	42.05	49.94	57.85
	Hot Spot Coefficient	1.19	1.15	1.18	1.18	1.15
15°C	Top layer oil temperature/ °C	33.97	39.00	46.41	53.72	62.39
	Hot Spot Coefficient	0.99	1.19	1.11	1.09	1.13
20°C	Top oil temperature /°C	37.99	43.60	49.82	57.30	65.43
	Hot Spot Coefficient	1.05	1.07	1.10	1.10	1.16
25°C	Top oil temperature/ °C	41.53	47.25	53.54	61.29	70.30
	Hot Spot Coefficient	1.00	1.03	1.08	1.08	1.14
30°C	Top oil temperature/ °C	46.39	51.36	57.78	65.42	74.36
	Hot Spot Coefficient	0.84	1.02	1.06	1.09	1.11
35°C	Top layer oil temperature/ °C	50.95	55.42	61.90	69.89	78.08
	Hot Spot Coefficient	0.76	1.02	1.06	1.08	1.14
40°C	Top layer oil temperature/ °C	55.17	60.05	66.45	73.49	83.19
	Hot Spot Coefficient	0.80	0.96	1.04	1.11	1.14

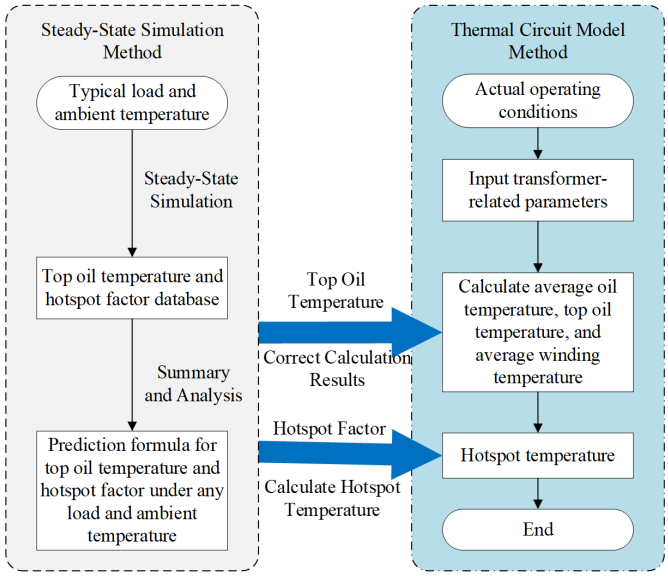

Figure 17. Coupling Calculation Flow

circuit model method needs to input the top oil temperature and hot spot coefficient of the current operating state obtained by the steady-state simulation method, the following Table 3 can be obtained by collating these data.

(2) In order to obtain the top oil temperature and hot spot coefficient of the transformer under any operating state, it is necessary to analyze the data obtained under typical operating conditions. The load loss is proportional to the square of the load factor, so the variation curve of the top oil temperature with the square of the ambient temperature and the load rate is respectively made, as shown in Fig. 18 below.

The top oil temperature increases with the increase of the square of the ambient temperature and the load rate, respectively, and shows a strong linear relationship, so the multiple linear regression method is used to analyze the change trend of the top oil temperature under any operating state. Multiple linear regression is a kind of regression analysis method, which is often used to study the relationship between dependent variables and multiple independent variables and has been widely used in various fields. A multiple linear regression equation is established based on the number of dependent variables, as shown in (19).

$$f(x) = a_0 + a_1 x_1 + a_2 x_2^2 \tag{19}$$

where x_1 and x_2 represent the ambient temperature and load rate, respectively, with the help of statistical analysis software SPSS, the estimated values of parameters a_0, a_1 and a_2 can be obtained through stepwise regression, so as to obtain the expression of the top oil temperature, as shown in the following ().

$$T_{\text{top-oil}} = 19.51 + 0.8x_1 + 21.76x_2^2 \tag{20}$$

In order to evaluate the effect of the regression model, the equation was tested for goodness-of-fit R_2 and significance F.R_2 is 0.997, which is very close to 1, and the F-value falls in the rejection domain, which is very significant, so the equation has a good linear regression effect.

The relationship between the hot spot coefficient and the ambient temperature and load rate is shown in Fig. 19 below, and the change of the hot spot coefficient is more complex than that of the top oil temperature. Overall, the hot spot coefficient is negatively correlated with the

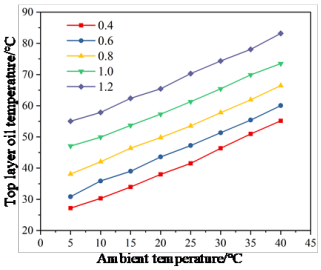

(a) The Variation Relationship of Top Layer Oil Temperature and Ambient Temperature Under Different Loading Rates

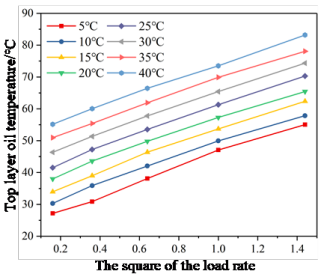

(b) The Variation Relationship of the Top Layer Oil Temperature and the Square of the Load Rate Under Different Environmental Temperatures

Figure 18. The Variation Law of the Top Layer Oil Temperature of the Transformer Under Different Operating Conditions

ambient temperature and positively correlated with the load rate, which is a nonlinear problem. If the nonlinear regression method is to be adopted, the difficulty lies in determining the nonlinear regression equation, considering that the change of the hot spot coefficient is approximately linear, and the linear fitting method is used to determine the expression.

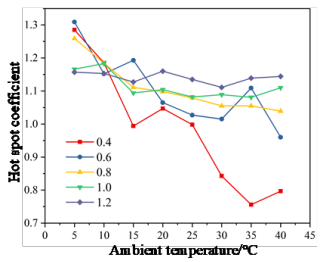

(a) The Relationship Between the Hot Spot Coefficient and the Variation of Ambient Temperature

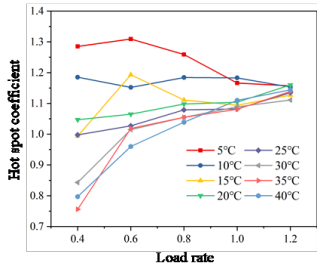

(b) The Relationship Between the Hot Spot Coefficient and the Square of the Load Rate

Figure 19. The Variation Law of the Transformer Hot Spot Coefficient Under Different Operating Conditions

Firstly, based on Fig.19(b) above, the hot spot coefficient H curve at different ambient temperatures is linearly fitted, and the expression is obtained as follows.

$$\begin{aligned}
H &= -0.20x_2 + 1.40x_1 \quad (x_1 = 5°\mathrm{C}) \\
H &= -0.017x_2 + 1.18x_1 \quad (x_1 = 10°\mathrm{C}) \\
H &= 0.084x_2 + 1.04x_1 \quad (x_1 = 15°\mathrm{C}) \\
H &= 0.13x_2 + 0.99x_1 \quad (x_1 = 20°\mathrm{C}) \\
H &= 0.16x_2 + 0.93x_1 \quad (x_1 = 25°\mathrm{C}) \\
H &= 0.31x_2 + 0.78x_1 \quad (x_1 = 30°\mathrm{C}) \\
H &= 0.41x_2 + 0.68x_1 \quad (x_1 = 35°\mathrm{C}) \\
H &= 0.42x_2 + 0.67x_1 \quad (x_1 = 40°\mathrm{C})
\end{aligned}$$

The slope and intercept of the equation at ambient temperature of 20°C are taken as the initial slope and initial intercept of the hot spot coefficient prediction equation, and the average value of the difference between the slope of the adjacent equation and the average value of the difference between the intercept are taken as the increase and decrease constants of the slope and intercept of the prediction equation, respectively, and the prediction equation is obtained:

$$H = \left[0.13 + \frac{0.089\,(x_1 - 20)}{5}\right] x_2 + \left[0.99 - \frac{0.10\,(x_1 - 20)}{5}\right] \tag{21}$$

Finishing type can get the following (22):

$$H = 1.40 - 0.02x_1 - 0.22x_2 + 0.018x_1x_2 \tag{22}$$

The goodness-of-fit test of the equation shows that R_2 is 0.823, and the predicted hotspot coefficient value of the equation is less than 0.1, so the coupled calculation model has good prediction accuracy.

The proposed field-path coupling model is used to calculate the average oil temperature, the average winding temperature, the top oil temperature and the hot spot temperature of a transformer under the operating conditions of temperature rise test conditions, and the calculation results are compared with the temperature rise test results, as follows.

The results are shown in the following table, where the definition of the average oil temperature in the temperature rise test value is the same as that of the previous two, and the average temperature value of the winding is the average value of the high-voltage winding and the average temperature value of the low-voltage winding. From the results in the table, it can be seen that the error of the calculated value of the field-path coupling model and the temperature rise test value is within 5°C, which can meet the actual engineering requirements.

According to the thickness of the transformer wire and the rated capacity, the hot spot coefficient $H = 1.2$ is determined, and the hot spot temperature value is 101.68°C according to the standard recommendation method. The simulation results show that the hot spot temperature of the transformer appears at the #1-line cake, that is, the #1 optical fiber temperature measurement point, so the temperature value of 115.0°C is used as the temperature rise test value of the transformer hot spot temperature for comparison. According to Table 4 below, the absolute error between the hot spot temperature value and the temperature rise test value calculated by the field-path coupling model is 0.25°C, while the error of the standard recommendation method is 14.32°C. The model has high calculation accuracy.

5. Conclusions

This paper deeply probes into the thermal characteristics and overload capacity of converter transformers in offshore wind power flexible DC transmission systems. Two main conclusions are drawn:

(1) By using Fluent to solve the 2D temperature and flow fields of the transformer, we studied the temperature-dependent variations in transformer oil's properties,

Table 4
Calculation Results of Test and Field-Path Coupling Method

Amount of contrast	**Calculated value** /°C	**Test values** /°C	**Absolute error** /°C	**Relative error** /%
Average oil temperature	49.80	49.65	0.15	0.30
Top layer oil temperature	65.26	64.90	0.36	0.55
Average temperature of the windings	75.74	75.60	0.14	0.19
Hot spot temperature	115.25	/	/	/

including density, specific heat capacity, thermal conductivity, and dynamic viscosity. These findings enhanced the precision of thermal field simulations. Detailed descriptions of solid domain material properties and heat source setups were provided, covering the physical properties of silicon steel, copper, and cellulose, as well as the heat flux density calculations for each low and high-voltage winding segment. Regarding boundary conditions and model selection, after considering the interaction between fluid and wall, suitable conditions and a laminar flow model for the oil flow within the transformer were chosen. Taking the DF-80000/220 transformer as an example, the internal temperature and oil flow velocity distributions were obtained. It was found that the hotspot temperature appears at the top of the low-voltage winding, the highest temperature of the high-voltage winding is in the top coil, and the maximum internal oil flow velocity occurs at the internal baffle.

(2) A field-circuit coupled calculation method is proposed. By analyzing the coupling parameters of the thermal circuit model and steady-state simulation, and refining the model parameters based on simulation results, the hot-spot temperature can be accurately calculated. Through steady-state simulation of the transformer's operation under typical load currents and ambient temperatures, a database of top-oil temperatures, bottom-oil temperatures, hot-spot temperatures, and average winding temperatures was formed, along with the calculation of the hot-spot coefficient. Based on the database, the variation laws of top-oil temperature and hot-spot coefficient with load ratio and ambient temperature were analyzed, leading to the development of formulas for calculating these parameters under any load and ambient temperature conditions. Finally, the calculated values of the field-circuit coupled model show an error of less than $5°C$ compared to the temperature-rise test values, meeting the practical engineering requirements. The absolute error of the calculated hot-spot temperature compared to the test value is $0.25°C$, which is smaller than that of the standard recommended method, indicating a higher calculation accuracy.

Funding

5500-202319103A-1-1-ZN Research on Key Technologies of Medium-Frequency Convergence DC Transmission for Large-Capacity Offshore Wind Power.

Acknowledgments

Thank you for the great assistance provided by TBEA Hengyang Transformer Co., Ltd.

References

[1] X. Zhou, Y. Luo, L. Zhu, J. Bai, T. Tian, B. Liu, Y. Xu, and W. Zhao, "Analysis of Fine Fault Electrothermal Characteristics of Converter Transformer Reduced-Scale Model," *Energies*, vol. 17, no. 5, 2024.

[2] Y. Wang, K. Liu, M. Lin, H. Tang, X. Li, and G. Wu, "Analysis of electrical–thermal-stress characteristics for eccentric contact strip in the valve-side bushing of converter transformer," *High Voltage*, vol. 10, no. 1, pp. 106–115, 2024.

[3] J. Peiyu, Z. Zhanlong, D. Zijian, W. Yongye, X. Rui, D. Jun, and P. Zhicheng, "Research on distribution characteristics of vibration signals of ±500 kV HVDC converter transformer winding based on load test," *International Journal of Electrical Power and Energy Systems*, vol. 132, p. 107200, 2021.

[4] P. Huang, T. Shen, Z. Liu, R. Dian, X. Wanlun, and D. Wang, "Thermal characteristics analysis of medium frequency transformer under multiple working conditions," *Thermal Science*, vol. 28, no. 1B, pp. 599–609, 2024.

[5] Z. Zhou, C. Luo, F. Zhang, J. Zhang, X. Yang, P. Yu, and M. Liao, "Thermal Management in 500 kV Oil-Immersed Converter Transformers: Synergistic Investigation of Critical Parameters Through Simulation and Experiment," *Energies*, vol. 18, no. 9, p. 2270, 2025.

[6] J. Peiyu, Z. Zhanlong, D. Zijian, Y. Yu, P. Zhicheng, Y. Fanghui, and Q. Menghao, "Transient-steady state vibration characteristics and influencing factors under no-load closing conditions of converter transformers," *International Journal of Electrical Power and Energy Systems*, vol. 155, p. 109497, 2024.

[7] Y. Guangyuan, L. Xingyuan, F. Ming, and L. Kuan, "Research on the Calculation Method of Overload Capacity of Converter Transformer," *Transformer*, vol. 52, no. 03, pp. 16–20, 2015. (in Chinese).

[8] W. Jian, W. Yi, X. Zhangmin, X. Xiaofu, and O. Jinxin, "Cooperative overload control strategy of power grid transformer considering dynamic security margin of transformer in emergencies," *International Journal of Electrical Power and Energy Systems*, vol. 140, p. 108098, 2022.

[9] "Thermal Overload Protection of Power Transformers," *Water and Energy Abstracts*, vol. 18, no. 2, pp. 57–57, 2008.

[10] H. Li, Q. Yao, and X. Li, "Voiceprint Fault Diagnosis of Converter Transformer under Load Influence Based on Multi-Strategy Improved Mel-Frequency Spectrum Coefficient and Temporal Convolutional Network," *Sensors*, vol. 24, no. 3, p. 757, 2024.

[11] L. Dong, "Analysis of temperature rise characteristics and calculation of overload capacity of converter transformer," *Electric Power Equipment Management*, no. 01, pp. 194–195, 201, 2021. CNKI:SUN:DSGL.0.2021-01-081.

[12] Q. Menghao, Y. Fanghui, Y. Yuan, J. Peiyu, W. Liming, and Z. Linjie, "Vibration characteristics of ±800 kV converter transformers part II: Under load conditions," *International Journal of Electrical Power and Energy Systems*, vol. 159, p. 110026, 2024.

[13] X. Jing, H. Jian, Z. Ning, L. Ruijin, F. Yun, L. Wenlong, and C. Huanchao, "Simulation study on converter transformer windings stress characteristics under harmonic current and temperature rise effect," *International Journal of Electrical Power and Energy Systems*, vol. 165, p. 110505, 2025.

[14] W. Hao, Z. Li, S. Youliang, and Z. Liang, "Research on the influence mechanism of harmonic components on the noise distribution characteristics of converter transformers," *International Journal of Electrical Power and Energy Systems*, vol. 160, p. 110095, 2024.

[15] A. Irshad and A. Z. J. Nadeem, "An Intelligent Technique for the Health Assessment of Power Transformer Using Thermal Imaging," *International Journal of Power and Energy Systems*, vol. 41, no. 1, pp. 48–57, 2021.

[16] S. A. Mehdi, "Flux-Based Transformer Model with Inter-Turn Fault Considering Saturation Effect," *International Journal of Power and Energy Systems*, vol. 40, no. 1, pp. 1–8, 2020.

Biographies

Zheng Zhao received his M.S. degree in Electrical Engineering from Xi'an Jiaotong University, Xi'an, China, in 2012. Since then, he has been Deputy Director of the HVDC Technology Consulting Center at the State Grid Economic Research Institute Co., Ltd. His research interests include HVDC, converter transformers, and other high-voltage electrical equipment.

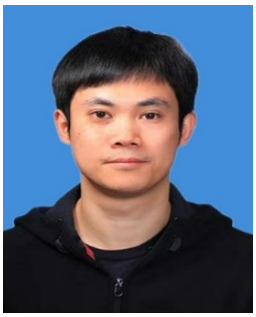

Lingfei Xiong received his Ph.D. degree in Electrical Engineering from North China Electric Power University, Beijing, China, in 2016. Since then, he has been Director of the Converter Station Department in the HVDC Technology Consulting Center at the State Grid Economic Research Institute Co., Ltd. His research interests include HVDC, converter transformers, and other high-voltage electrical equipment.

Kuan Zheng received the PhD degree in Electrical Engineering from Tsinghua University, Beijing, China, in 2019. She is currently employed at State Grid Economic Research Institute Co., Ltd. Her research interests include HVDC, Converter transformers and other high-voltage electrical equipment.